NANO · MICRO small
www.small-journal.com

Sodium Niobate Nanowires Embedded PVA-Hydrogel-Based Triboelectric Nanogenerator for Versatile Energy Harvesting and Self-Powered CO Gas Sensor

Monical Jaiswal, Shivam Singh, Bharat Sharma, Sumit Choudhary, Robin Kumar, and Satinder K. Sharma*

The surging demand for sustainable energy solutions and adaptable electronic devices has led to the exploration of alternative and advanced power sources. Triboelectric Nanogenerators (TENGs) stand out as a promising technology for efficient energy harvesting, but research on fully flexible and environmental friendly TENGs still remain limited. In this study, an innovative approach is introduced utilizing an ionic-solution modified conductive hydrogel embedded with piezoelectric sodium niobate nanowires-based Triboelectric Nanogenerator (NW-TENG), offering intrinsic advantages to healthcare and wearable devices. The synthesized NW-TENG, with a 12.5 cm^2 surface area, achieves peak output performance, producing ≈840 V of voltage and 2.3 µC of charge transfer, respectively. The rectified energy powers up 30 LEDs and a stopwatch; while the NW-TENG efficiently charges capacitors from 1µF to 100 µF, reaching 1 V within 4 to 65 s at 6 Hz. Integration with prototype carbon monoxide (CO) gas sensor transform the device into a self-powered gas sensory technology. This study provides a comprehensive understanding of nanowire effects on TENG performance, offering insights for designing highly flexible and environmentally friendly TENGs, and extending applications to portable self-powered gas sensors and wearable devices.

1. Introduction

The advancements in the field of flexible electronics, distinguished by their exceptional reliability and deformability, have facilitated the emergence of novel applications such as foldable displays, touch sensors, wearable devices, and epidermal electronics.[1–5] However, the extensive utilization of contemporary electronic devices poses a considerable environmental threat owing to their non-degradable or non-recyclable characteristics. Consequently, there is a growing emphasis on the development of electronic materials that exhibit high biodegradability and biocompatibility.[6–8] The progress in flexible and environmental friendly electronics has presented substantial challenges for conventional power sources,[9–11] underscoring the need for the development of eco-friendly power generators capable of powering these emerging technologies.[12]

In recent times, there has been a concerted effort to fabricate stretchable Triboelectric Nanogenerators (TENGs) using diverse methodologies. For instance, Wang et al. introduced an innovative multilayer elastomeric TENG with closely stacked arches as fundamental functional units.[13] Similarly, Sun et al. devised a transparent and stretchable wrinkled PEDOT:PSS electrode-based TENG capable of achieving a maximum strain of ≈100%.[14] Zhai et al. studied ZnS and Cu mixed PDMS layers over Cu coil to fabricate TENG for energy harvesting.[15] Different polymers have been explored for the fabrication of efficient TENG.[16,17] These devices exhibit exceptional practical properties for energy harvesting from bodily motion, attributable to their material and structural advancements. However, the power output performance of the majority of existing stretchable devices is constrained, typically registering lower than 100 V, primarily due to low surface roughness. Additionally, the high and variable resistance of these devices can significantly influence electron transmission at the interface, resulting in low current.[5,18,19] To augment surface charge density and attain relatively high-output TENGs, micro/nanostructures have been engineered on the surfaces of triboelectric materials.[19] Over the past decade, various studies have demonstrated that electrospinning nanofibrous membranes constitute an effective method for enhancing the performance of TENGs.[20] Electrospinning, being a simple, straightforward, economical, and versatile approach, is employed for fabricating nanostructured films from different polymer materials.[21] Electrospun nanofibrous membranes offer advantages such as high specific surface area,

M. Jaiswal, S. Singh, R. Kumar
Amity University
Noida, UP 201313, India
E-mail: rkumar5@amity.edu
B. Sharma
Karlsruhe Institute of Technology
Kaiserstraße 12, 76131 Karlsruhe, Germany
S. Choudhary, S. K. Sharma
Indian Institute of Technology (IIT) Mandi
Mandi, Himachal Pradesh 175075, India

The ORCID identification number(s) for the author(s) of this article can be found under https://doi.org/10.1002/smll.202403699

DOI: 10.1002/smll.202403699

extraordinarily high surface roughness, and good flexibility owing to their micro/nanostructure.[22] It renders them highly promising in the development of high-performance TENG applications.[23] However, electrospun films exhibit notable drawbacks, primarily their flexibility rather than stretchability. This limitation stems from the use of an aluminum foil substrate in electrospray spinning, which lacks adequate adhesion between the base film and the electrospun layer despite possessing good electrical conductivity.

Hydrogels exhibit numerous advantageous characteristics, including high softness, rapid diffusion, flexibility, elasticity, biodegradability, and biocompatibility. These attributes position them as excellent candidates for deployment as electrostatic electrodes in TENGs, in contrast to other conductive materials.[24–26] As promising flexible ionic conductors, hydrogel-based TENGs have found application in energy harvesting and self-powered sensors.[27–30] Nevertheless, conventional hydrogels encounter rigidity, brittleness, and poor conductivity challenges, primarily stemming from the significant water content inherent in these materials. It is crucial to highlight that the performance of hydrogel-based TENGs relies on a unique combination of quasi-solid mechanical behavior and quasi-water transport properties intrinsic to these hydrogels. However, the qualities like flexibility and strectability are compromised at low temperatures, especially sub-zero levels. It attributes to the fact that water-based conductive hydrogels invariably lose their elasticity under such cold conditions.[31] For example, the cold environments experienced during winter or polar expeditions pose significant obstacles to the widespread utilization of TENGs as universal power sources.

This article introduces a pioneering Hydrogel-based triboelectric nanogenerator (TENG) characterized by full flexibility and environmental friendliness. The design employs physically cross-linked Polyvinyl Alcohol (PVA) hydrogel. The standard hydrogel comprises $NaNbO_3$ nanowires embedded in the hydrogel (NW-TENG), with a Silicone rubber layer affixed above and below with an integrated stainless steel (SS) wire mesh as electrode. At a load resistance of 1 MΩ, the peak output power for our device attains 0.08 W and 11.8 W m^{-2} at the load of 42 MΩ. Our presented flexible NW-TENG demonstrates the capability to generate an open-circuit voltage (V_{oc}) of ≈ 840 V, short-circuit current (I_{sc}) of ≈ 276 μA, and short-circuit transferred charge (Q_{sc}) of ≈ 2 μC. The versatility of this work is showcased through applications of NW-TENG as power source for illuminating LEDs and charging capacitors for wearable electronics. Beyond these applications, we present proof-of-concept wearable NW-TENG sensors capable of real-time monitoring of human motion and sensing CO gas in the environment. This work marks a compelling advancement in the realm of high-output performance and self-healing capability in flexible TENGs, displaying promising potential in diverse applications, including soft robots, smart artificial skins, wearable electronics, and human-machine interaction. Furthermore, using biodegradable PVA hydrogels in our prototype design opens avenues for recyclability, offering advantages such as environmental friendliness and cost-effectiveness to the Hydrogel-TENG technology.

2. Results and Discussion

Sodium niobate nanowires were synthesized using Niobate pentaoxide (Nb_2O_5) and Sodium hydroxide (NaOH) by reflux method.[32] The resulting nanowires exhibited a distinctive wire/rod-like structure, as evidenced by the SEM image inset of **Figure 1**a (i), EDS study is given in the supplementary file (Figure S1, Supporting Information). These $NaNbO_3$ nanowires, previously studied for their piezoelectric properties,[33–35] were then incorporated into a conductive hydrogel to augment the performance of Triboelectric Nanogenerators (NW-TENG). Figure 1b(i),(ii) demonstrates the successful dispersion of nanowires within the hydrogel matrix, while Figure 1b(iii) provides insight into the self-aligned arrangement of nanowires within the hydrogel. To further enhance the population of mobile ions (Na^+ and Cl^-) in the hydrogel, it was immersed in an aqueous NaCl solution (230 mM) for 60 minutes; during this process, hydrogel absorbs the ions.[36,37] These ions will provide high output performance of NW-TENG. Detailed explanation of the role of ionic solution in the mechanism is discussed in supplementary file (Figure S5, Supporting Information). Subsequent EDX analysis of the hydrogel confirmed the presence of sodium (Na) and chlorine (Cl), indicating the successful incorporation of ions into the hydrogel (Figure S1, Supporting Information). Furthermore, the robustness of the hydrogel was assessed under various deformations, highlighting its exceptional stretchability and foldability. Images depicting the hydrogel's response to different deformations underscore its endurance. The electrical resistance of the hydrogel exhibited an increase during stretching, rising from 0.88 MΩ to 1.21 MΩ upon 100% stretching. This behavior positions the hydrogel as a promising piezo-resistor, as illustrated in Figure 1c.

The NW-TENG device was assembled by packaging the NW-hydrogel composite between two layers of silicone rubber (1 mm each), serving as triboelectrification layers. It is reported that thin triboelectrification layers result in higher output voltage.[38,39] Notably, copper and aluminum were deliberately avoided for the electrodes, as their corrosion in the presence of water and the formation of oxides could compromise the durability and performance of the NW-TENG. Instead, a mesh of stainless steel (SS) wires was utilized, as depicted in **Figure 2**b. This choice aimed to mitigate corrosion-related issues and ensure sustained performance over time. The SS electrode used was also tested for robust bending in upward and downward directions repeatedly and change in its resistance was studied, results are discussed in supplementary file (Figure S4, Supporting Information). The operational mechanism of the NW-TENG is elucidated in Figure 2a, delineating the stepwise processes involved in its functioning. In this configuration, the silicone rubber layers serve as negative triboelectric materials, while human skin acts as the positive triboelectric layer. The NW-TENG operates based on the coupled effects of triboelectrification and electrostatic induction,[29] modulated by the piezoelectric properties of $NaNbO_3$ nanowires. During the operational cycle, when a pressure force is applied to the NW-TENG by a bare human hand in STATE I, the force is transmitted through the silicone layer to the nanowires, subsequently

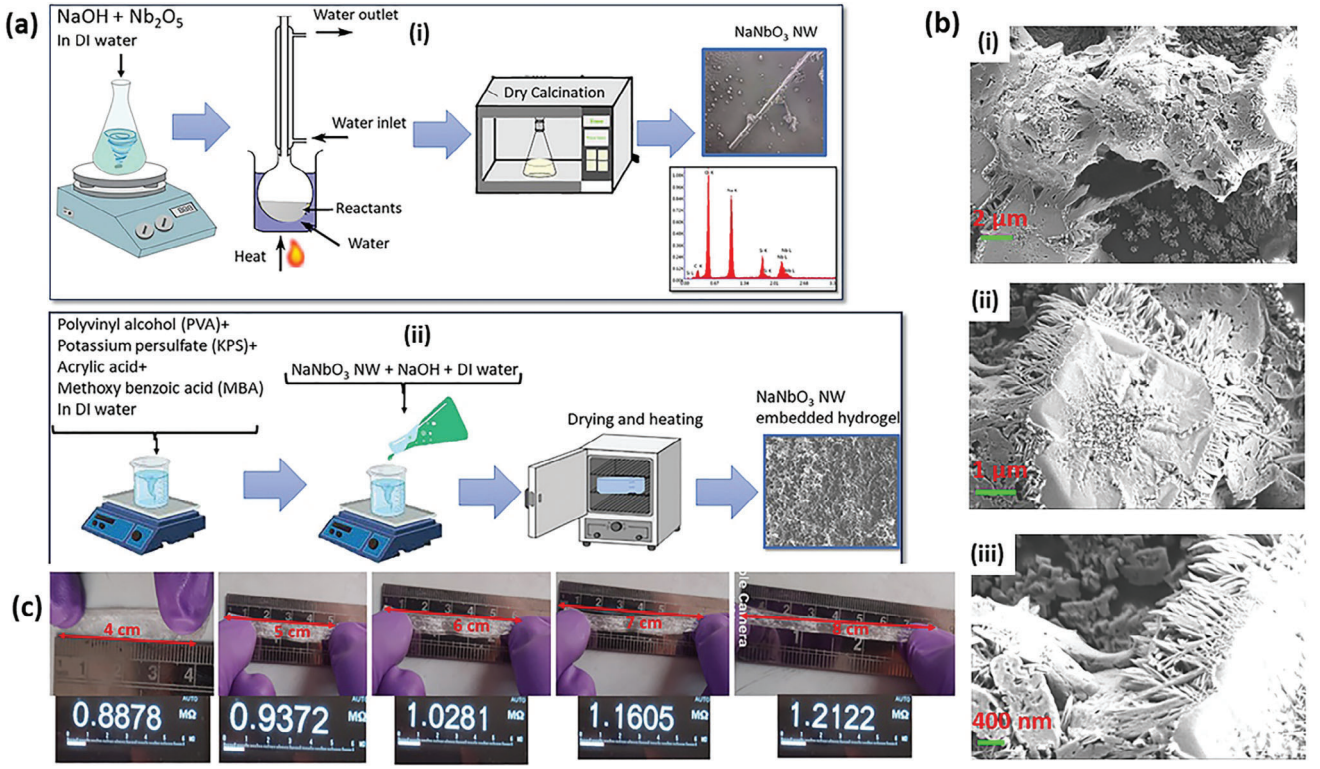

Figure 1. a) Synthesis method of (i) sodium niobate nanowires and (ii) $NaNbO_3$ nanowires embedded hydrogel b) SEM image of $NaNbO_3$ NW embedded hydrogel (i), (ii), (iii) showing the presence and alignment of nanowires in hydrogel c) Flexibility of NW embedded hydrogel.

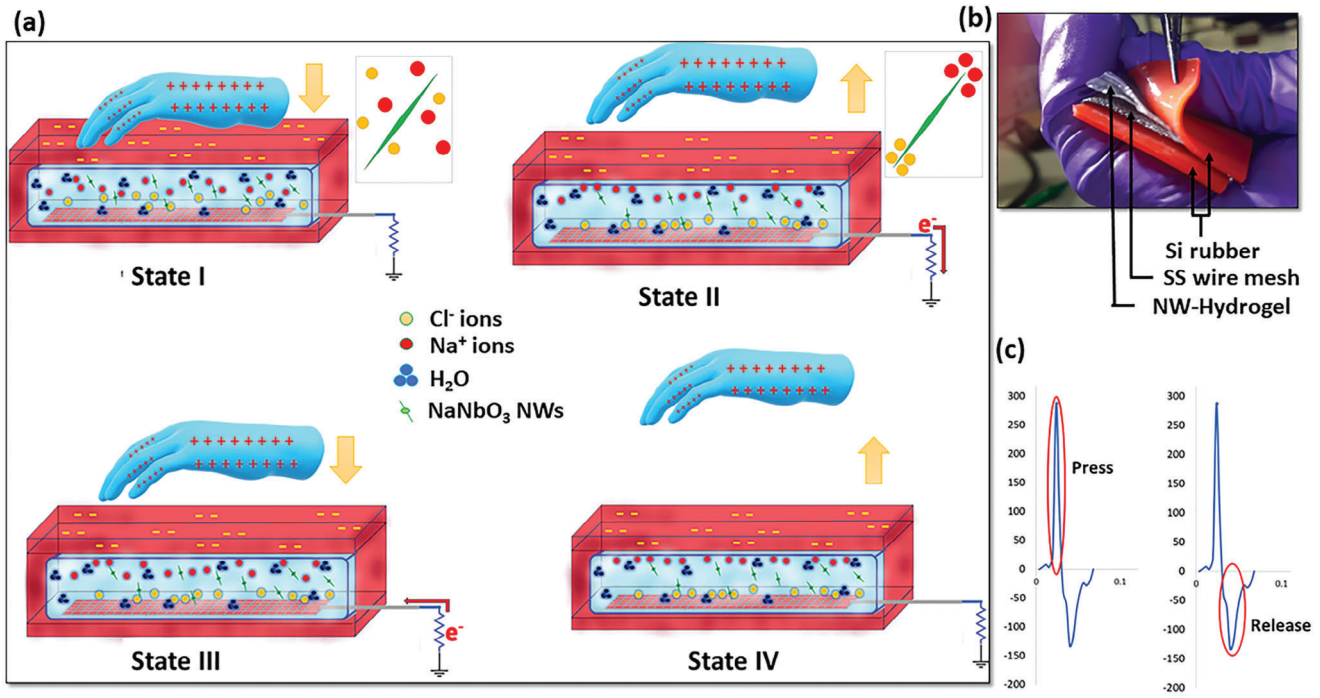

Figure 2. a) Schematic working mechanism of NW-TENG b) Fabrication of NW-TENG c) Press and release response of NW-TENG upon hitting with bare hand.

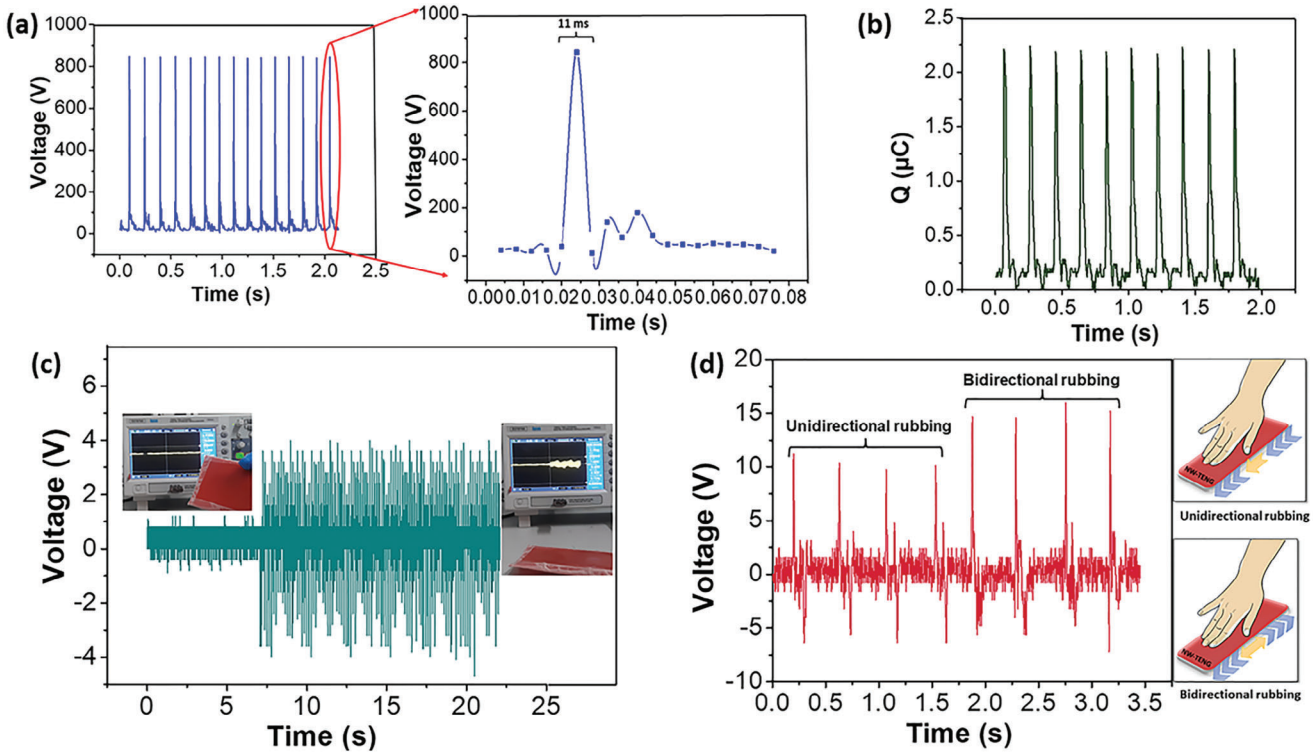

Figure 3. a) Open circuit voltage (V) at beating frequency of 6 Hz b) Charge transfer c) Response of NW-TENG in respect to table vibration and in static state d) open circuit voltage during rubbing by bare human hand in one direction and bidirectional.

instant polarizing the nanowires within the hydrogel. This polarization induces the separation of ions in the hydrogel, increasing the population of mobile ions [40,41] (as shown in the inset of Figure 2a). Simultaneously, charges transfer from the skin to the silicone rubber, rendering the silicone rubber layer negatively charged.

As the hand moves away in STATE II, the negative charge accumulated on the silicone rubber attracts ambulant Na^+ ions toward the interface, creating a Na^+ ion-rich interface. Concurrently, the interface between SS wires and hydrogel becomes polarized, resulting in the formation of electric double layers on each wire. The mesh of SS wires provides a high surface area and numerous interfaces for higher negative charge (Cl^-) accumulation. Consequently, a higher number of negative ions (Cl^-) gather at the SS wires, and to balance the static charge, electrons flow toward the ground until equilibrium is achieved (STATE III). When the hand approaches NW-TENG again in STATE IV, electrons flow back to the SS wires and hydrogel interface from the ground. Upon physical contact between the hand and silicone rubber, the charge distribution returns to its initial state, completing the operational cycle. This cyclic process illustrates the functioning of the NW-TENG, wherein mechanical energy from the applied pressure is converted into electrical energy through the triboelectric and piezoelectric effects.

The contribution of nanowires to high-output performance becomes apparent, with continuous beating potentially aligning more nanowires and further enhancing the output voltage, as depicted in **Figure** 3a. The device's capability for generating continuous electrical power through repeated beating was demonstrated by evaluating a 12.5 cm^2 NW-TENG subjected to beating at a frequency of 6 Hz with a force of 2.45 N. The maximum open-circuit voltage (V_{oc}) and transferred charge (Qtr) remained consistently near 840 V ± 20 V and ≈2.3 μC, respectively as shown in Figure 3a,b. A pulse width of 11 ms accompanied by a peak voltage of 840 V was observed (Response of NW-TENG against mechanical stimuli are given in supplementary movies). Remarkably, the presented NW-TENG exhibited superior output performance, surpassing previously reported single-electrode mode stretchable TENGs in power, charge transfer, and peak output voltage, as summarized in **Table** 1.

Ambient vibrations were leveraged to assess the NW-TENG's output performance, as illustrated in Figure 3c. Holding the NW-TENG in hand produced a V_{oc} of ≈0.7 V, while placing it on a table increased V_{oc} to ≈3.5 V. This sensitivity to minute vibrations suggests potential applications in energy harvesting from ambient vibrations. Notably, table vibrations, though faint, influence the contact area between the table surface and the silicone layer, inducing triboelectrification. In contrast, vibrations from the human hand have negligible effect compared to table vibrations, resulting in negligible output. To further evaluate the NW-TENG's performance, the cell's surface was gently rubbed in one direction and then back and forth. The results presented in Figure 3d show that rubbing in one direction alone produced a V_{oc} of ≈9–10 V, while continuous rubbing in both directions increased V_{oc} to ≈15–16 V. The relatively lower output in the former case could be attributed to the non-polarization of nanowires, highlighting the nuanced influence of the rubbing direction on the device's performance.

Table 1. Comparative study of TENGs consisting polymer based hydrogels.

S.N.	Material	Max. Output voltage	Power density	Refs.
1	PDMS, PAM hydrogel	71V	0.135 W m^{-2} (800MΩ)	[25]
2	PVA/polydopamine/CNT hydrogel	95V	0.750 W m^{-2} (500MΩ)	[29]
3	PVA hydrogel, silicon rubber	50V	4×10^{-5} μW cm^{-2} (1MΩ)	[42]
4	PVA/PEI hydrogel, PDMS	70V	2.79 W m^{-2} (150MΩ)	[43]
5	PVA and sodium alginate (SA)	203 V	0.98 W m^{-2} (4.7 MΩ)	[44]
6	PVA hydrogel and PDMS film	200 V	0.002 mW (10 MΩ)	[45]
7	PVA hydrogel and MXene	180 V	0.33 W m^{-2} (1000 MΩ)	[46]
8	PVA hydrogel with NaCl	49 V	–	[36]
9	PVA/P(AM-co-AA)-Fe_3^+	238 V	0.27 W m^{-2} (300 MΩ)	[47]
10	Polyvinyl alcohol/phytic acid (PVA/PA) hydrogel	201	1.33 W m^{-2} (500 MΩ)	[48]
11	$NaNbO_3$ nanowires embedded PVA hydrogel	840 V	11.8 W m^{-2} (42 MΩ)	This work

The NW-TENG exhibits remarkable capabilities in discerning various human hand motions, as shown in **Figure 4a**; output V_{oc} upon tapping the cell from both sides (like clapping), keeping NW-TENG in between the hands and beating, showed almost similar pulses as press and release, maximizing the output performance. With different bending angles of knuckle joint and fingers, the peak amplitude of the open-circuit voltage changed. As depicted in Figure 4b, a linear association between the V_{oc} and the bending angle is recorded, highlighting the NW-TENG's potential as a bending angle sensor. The device's dimensions can be adjusted to enable the detection of human motion in different body parts. Notably, the NW-TENG proves effective in recognizing differences in bending angles between the knuckle and finger joints, showcasing the versatility of the device. Changing the bending angle from 180° to 100° results in a corresponding increment in open-circuit voltage from 20 to 80 V. To assess the NW-TENG's suitability as a force sensor, the device's output was recorded during controlled drops from heights of 5 cm, 10 cm, and 15 cm (Figure 4c). The calculated forces experienced by the NW-TENG during the falls were 0.0049 N, 0.0098 N, and 0.0147 N, respectively. The observed relationship between the output voltage (V_{oc}) and falling height was linear, with V_{oc} values of 15 V, 25 V, and 35 V, suggests the NW-TENG's potential application as a force sensor.

Figure 4d explores the effect of contact area on the V_{oc} of the NW-TENG (upon gentle touching) utilizing a device with an area of 30 cm^2 for the study. The results reveal a linear increase in V_{oc} with an expanded contact area between the NW-TENG cell and the electropositive material (nitrile pad). V_{oc} values of 40 V, 58 V, 81 V, and 138 V are obtained for contact areas of 6 cm^2, 14 cm^2, 20 cm^2, and 25 cm^2, of nitrile pad's respectively. This correlation suggests that a larger contact area facilitates greater charge transfer, contributing to higher V_{oc} values.

To assess the output power of the NW-TENG, different resistance values were connected as loads to an external circuit. The manipulation of external load resistance from 1 MΩ to 50 MΩ resulted in observable variations in the V_{oc} and short-circuit current (I_{sc}), as depicted in **Figure 5a**. The relationship between power (W) and applied load resistance is illustrated in Figure 5b, revealing that the output power reaches a maximum value of ≈0.08 W at a load resistance of 1 MΩ. The power (P = IV) calculation, where V is the output voltage and I is the output current density across the external load, is employed to determine power density. In a demonstration of its practical utility, the NW-TENG successfully powered 30 commercial LEDs connected in series through a continuous beating at a constant force, as depicted in Figure 5d (Movie S7-S10, Supporting Information).

Figure 5c presents the output stability of the NW-TENG over 8 weeks in ambient conditions (14^0C–27^0C). The output was monitored daily, and the results show that after the second week, a slight decrease of 6% was observed, stabilizing thereafter from the third week onward. This decline in output voltage may be attributed to potential water leakage from the hydrogel due to continuous beating, emphasizing the importance of environmental factors in the long-term stability of the NW-TENG.

A bridge rectifier was incorporated into the system to harness the electrical energy generated by the NW-TENG, as depicted in Figure 5d. The evaluation of charging performance involved the application of various capacitors, and the accumulated energy was deployed to supply power to compact electronic devices, such as a digital watch and LEDs. The NW-TENG demonstrated effective charging across a spectrum of capacitors ranging from 1 to 100 μF, as delineated in **Figure 6a**. Notably, a NW-TENG with an area of 12.5 cm^2 achieved the charging of a 1 μF capacitor to 1 V in less than 4 seconds, while the same voltage was reached for a 100 μF capacitor in 64 seconds. Figure 6a provides detailed

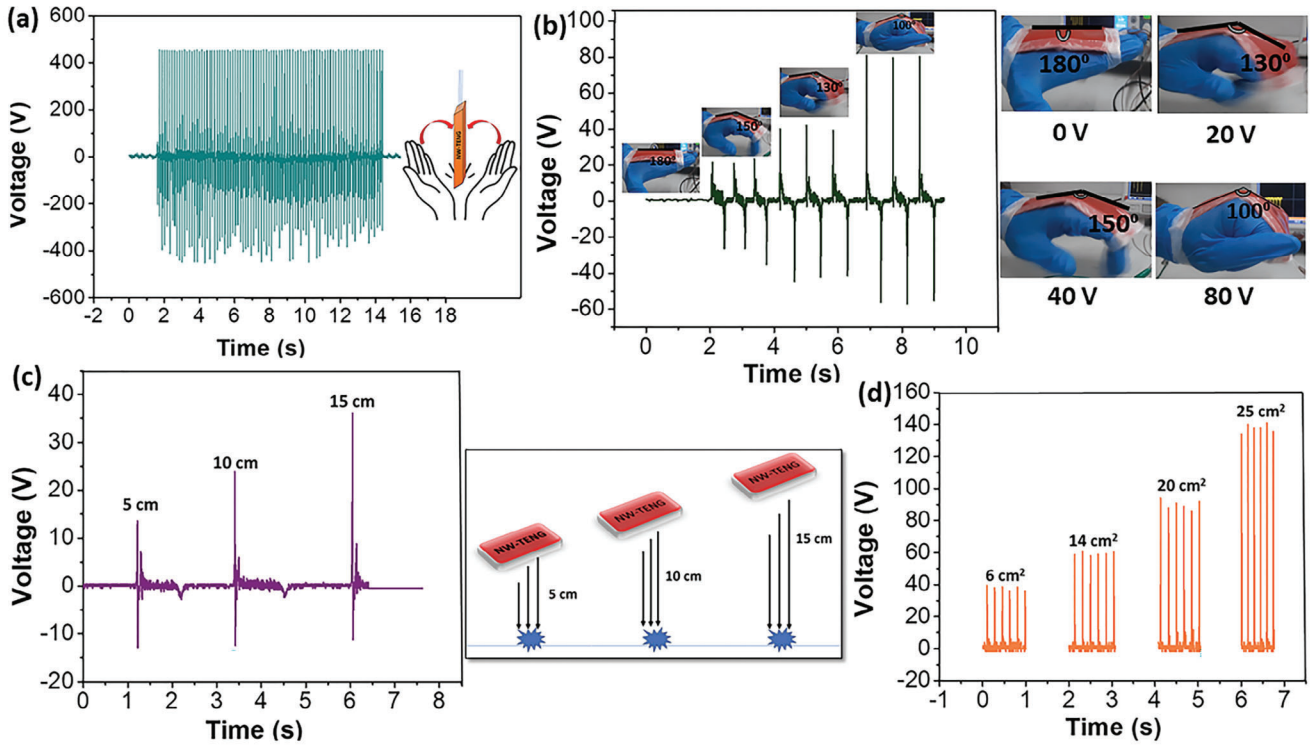

Figure 4. a) Response of NW-TENG upon tapping from both sides (Clapping) b) Output performance of NW-TENG on bending it from 180^0 to 100^0 c,d) energy harvesting performance of NW-TENG in various conditions (impact and contact area).

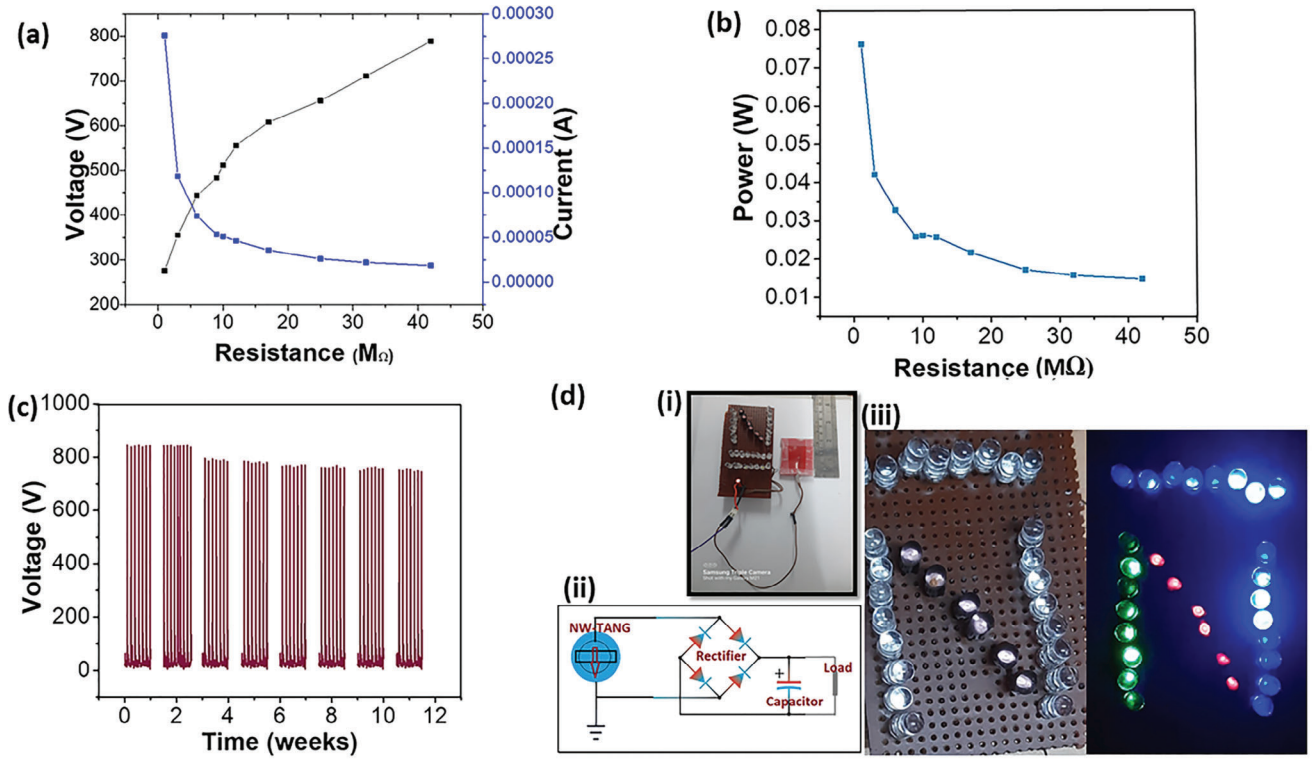

Figure 5. a) Output voltage and current versus the resistance of the external loads resistance b) Power output of NW-TENG for load resistance variation c) Repeatability of NW-TENG over 8 weeks under ambient conditions d) Circuit diagram for powering up 30 LEDs and the optical image of 30 LEDs powered by the NW-TENG.

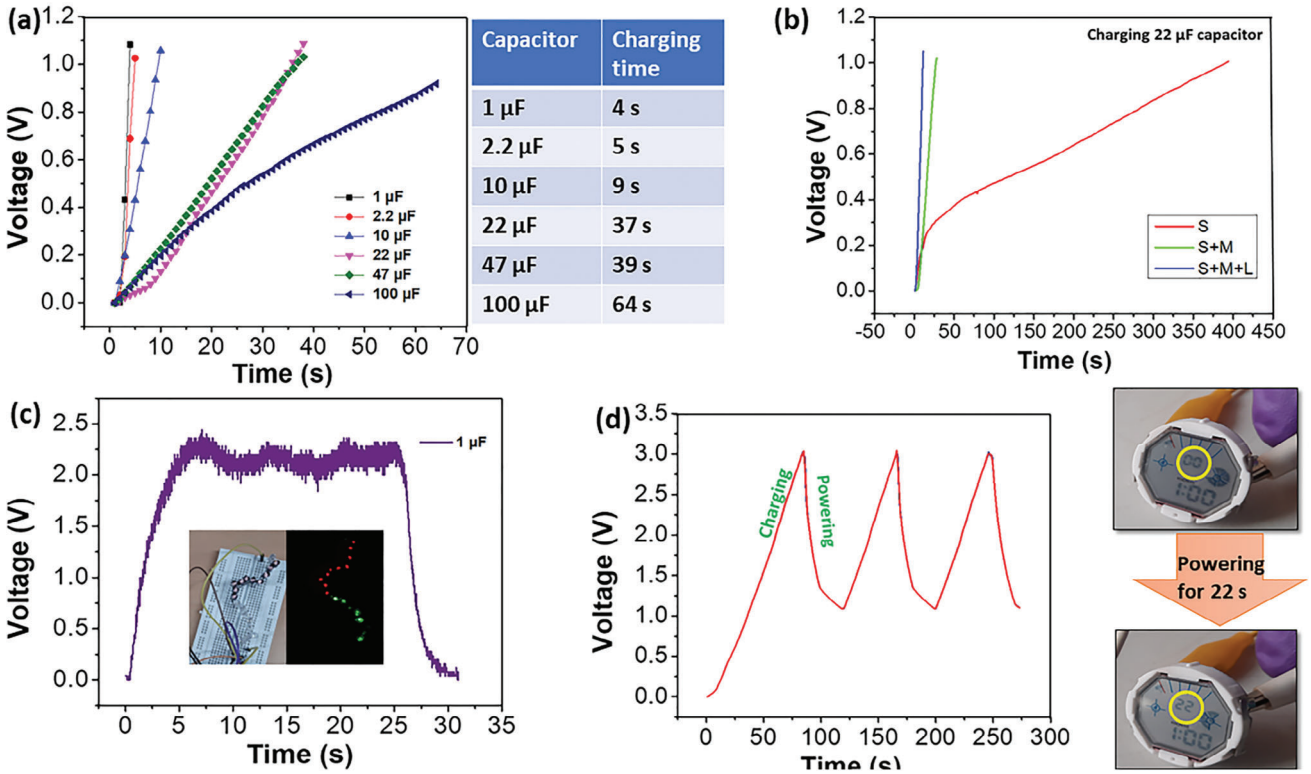

Figure 6. Demonstration of NW-TENG for energy conservation a) NW-TENG of 12.5 cm^2 area charging capacitors (1 µF, 2.2 µF, 10 µF, 22 µF, 47 µF, and 100 µF) up to 1 V b) Cumulative performance of NW-TENG cells of three different sizes (S-3 cm^2, M-12.5 cm^2, and L-49 cm^2) c) Capacitor charging and discharging during glowing 20 LEDs d) Voltage real-time charge/discharge profile of a 22 µF while running a digital watch using self-charging mode.

information on the charging times for each capacitor. To assess the scalability of the NW-TENG, devices of different sizes (S, M, and L@NW-TENG) with areas of 3 cm^2, 12.5 cm^2, and 49 cm^2, respectively, were fabricated. Figure 6b demonstrates that the S@NW-TENG (S) required 390 s to charge a 22 µF capacitor up to 1 V. However, when S and M@NW-TENG (M) and S, M, and L@NW-TENG (L) were connected in parallel for the charging of a 22 µF capacitor, the charging time was reduced to 33 seconds and 9 seconds, respectively. This cumulative charging effect underscores the significant acceleration of energy harvesting achievable through a parallel NW-TENG configuration.

Figure 6c illustrates the real-time charging and discharging of a capacitor while simultaneously powering 20 LEDs connected in series. The LEDs illuminated within 4 seconds, and with sustained mechanical beating, they continued to glow consistently while maintaining a constant capacitor voltage. The capacitor discharged in 5 s after the cessation of mechanical beating. As shown in Figure 6d, the energy stored in a 22 µF capacitor powered a digital watch for 22 s when charged to ≈3 V (in ≈75 s) by the NW-TENG. The charging and discharging cycles are depicted, and when the capacitor voltage drops to 1.4 V, the watch is temporarily dimmed, necessitating periodic recharging for sustained powering. For extended power supply, a 1000 µF capacitor was utilized, requiring ≈22 min to charge to 2 V. This output electrical energy proved sufficient to power a watch for over 15 minutes. These demonstrations affirm the NW-TENG's efficient conversion of mechanical motion into electrical energy, enabling the effective powering of small devices. The high flexibility of the NW-TENG positions it as a promising device for various applications in green mechanical energy harvesting. Additionally, the energy output can be further enhanced by increasing the NW-TENG's area or by stacking multiple NW-TENGs in a parallel configuration. Thus, the NW-TENG presented in this study emerges as a promising device for portable and self-powered next-generation devices.

2.1. Self-Powered CO Gas Sensing

The integration of NW-TENG with a CO gas sensor was undertaken to develop a self-powered gas sensor system. The chosen CO gas sensor is a resistive sensor composed of a thin film of copper-doped octahedral molecular sieves of potassium permanganate (OMS-2) (Cu-OMS-2).[29] The sensor's resistance decreases proportionally with the increasing concentration of CO gas. The sensor element was incorporated into a customized gas sensing setup (**Figure** 7a), and the voltage across the sensor element was systematically recorded at various concentrations of CO gas. For autonomous sensor operation, the NW-TENG was integrated into the system (Figure 7a), tapping into its mechanical energy. The NW-TENG was manually tapped at a frequency of ≈3 Hz, and the resultant voltage across the sensor element was documented.

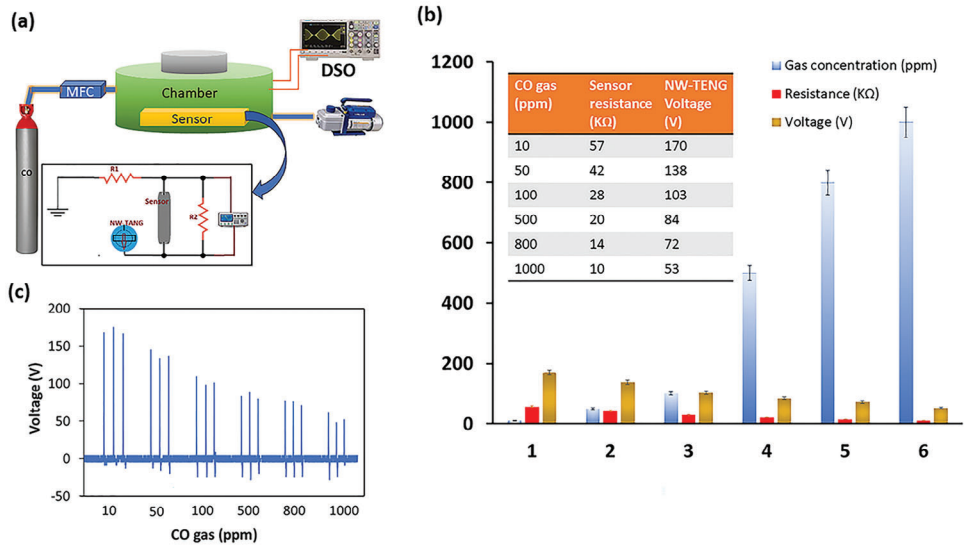

Figure 7. a) Circuit diagram for CO gas sensing using NW-TENG and Schematic presentation of gas sensing set up b) Voltage response of sensor integrated with NW-TENG with respect to CO gas concentration c) Output performance of NW-TENG in presence of increasing CO gas concentration.

The recorded data indicated a voltage drop to 53 V at a CO concentration of 1000 ppm, whereas the voltage surged to 170 V at 10 ppm of CO gas. Figure 7b visually represents the linear relationship between CO gas concentration and the output voltage of the NW-TENG. This observation underscores the potential application of NW-TENG in the realm of self-powered and autonomous gas sensing technology with mechanical tapping providing a sustainable power source for continuous and reliable operation.

3. Conclusions

In summary, this research focuses on innovative hydrogel-based triboelectric nanogenerators (NW-TENGs) that address critical challenges in flexible and environmental friendly electronics. Hydrogels embedded with sodium niobate nanowires ($NaNbO_3$ NWs) were used as the substrate material and sodium niobate nanowires were embedded within the hydrogel to create an environmentally friendly and fully flexible power generator. A combination of the hydrogel's stretchability, folding, and biodegradability, as well as $NaNbO_3$ NW's unique piezoelectric characteristics, contribute to the excellent performance of the device. In addition to harvesting energy from ambient vibrations, human motion, and even self-healing functions, the NW-TENG demonstrated extraordinary energy harvesting capabilities. Electrodes made from stainless steel wires mitigate corrosion problems, ensuring long-term performance. This device has shown versatility as a bending angle sensor and force sensor, suggesting that it could be used in wearable technologies and human-machine interaction. Its impressive output power also enabled it to power LED arrays and charge capacitors of various sizes efficiently. Scalability was demonstrated by parallelizing several devices, which accelerated energy generation significantly. The NW-TENG coupled with an autonomous CO gas sensor, demonstrated its potential for autonomous and energy-efficient gas sensors.

In terms of soft robotics, smart artificial skins, and wearable electronics, the research marks a significant advance in triboelectric nanogenerators that are powerful, flexible, and environmentally friendly. By developing prototype electronic devices with biodegradable PVA hydrogels demonstrates our commitment to sustainability and environmental responsibility. We now have a method to integrate self-powered, flexible electronics into our lives with the TENG technology presented. This technology not only addresses current challenges, but also opens up new possibilities for the integration of these devices into our everyday lives.

4. Experimental Section

Materials and Reagents: Analytical reagent grade Niobium pentoxide (Nb_2O_5) (3.74 M), NaOH pellets, NaCl, Poly-vinyl alcohol (PVA) acrylic acid ($C_3H_4O_2$), N, N-methylenebis acrylamide (MBA), and potassium persulfate (KPS) were purchased from Merck. Silicone rubber and SS wire mesh were procured from a local supplier. All materials are used without any further treatment.

Preparation of Sodium Niobate NWs: A solution denoted as solution A was prepared by combining Niobium pentoxide (3.74 M) and Sodium hydroxide (0.24 M) in 20 mL of deionized water. The mixture was thoroughly and vigorously stirred for 20 min to achieve a homogeneous solution. Subsequently, the resulting solution underwent reflux at a temperature of 120 °C for 3 h. Following the reflux process, the solution was allowed to cool down to room temperature and then subjected to filtration. The obtained powder underwent multiple washes with deionized water and was subsequently dried at 100 °C in a convection oven.

The resulting powders were then placed into a quartz crucible and subjected to annealing at 400 °C in a muffle furnace, as depicted in Figure 1a(i). The outcome of this thermal treatment was the production of a white-colored powder identified as Sodium Niobate ($NaNbO_3$) nanoparticles. This multistep process involving mixing, refluxing, filtration, washing, drying, and annealing was instrumental in obtaining the desired nanomaterial with the intended composition and properties.

Preparation of Hydro Gel: To prepare Solution B, 10 grams of polyvinyl alcohol (PVA) were dissolved in 250 mL of hot double-distilled water at 60 °C. Subsequently, a predetermined quantity of acrylic acid (C3H4O2 – 43.7 мм*100), N, N-methylenebis acrylamide (MBA – 19.45 мм), and

potassium persulfate (KPS – 11.1 mM) was added to Solution B. The resulting mixture, denoted as Solution C, underwent stirring for 10 min. In a separate step, Sodium Niobate nanoparticles and NaCl (250 mM), dispersed in 5 mL of double-distilled water (DDW), were introduced into Solution C. The entire mixture was further stirred for 30 minutes at room temperature (30 °C), following the procedure outlined in Figure 1a(ii).

The reaction mixture was then homogenized in a glass mold made of Borosil glass and maintained at 35 °C for 24 h. The outcome of this process was the formation of a thin semi-transparent film, which exhibited the incorporation of Nb nanowires. This synthesis procedure involving the sequential preparation of Solution B, the addition of specific components, and subsequent homogenization led to the successful fabrication of the desired film structure with embedded Nb nanowires.

Preparation of Power Generator Cell (NW-TENG): The hydrogel sheet containing embedded Nb NWs, which was previously prepared, underwent immersion in deionized water for 60 min. Subsequently, the hydrogel sheet was cut into dimensions of 5 cm x 2.5 cm x 0.2 cm and carefully packaged between two layers of silicone rubber, each with a thickness of 1 mm. To establish electrical conductivity, a stainless steel (SS) wire mesh was affixed to the hydrogel as a conductor. The entire assembly, comprising the hydrogel sheet, SS wire mesh, and silicone rubber layers, was securely sealed using epoxy to ensure structural integrity and prevent water ingress. This encapsulation process resulted in the creation of a compact and well-protected device ready for further applications or testing.

Characterizations: The morphology and elemental composition analysis of the obtained Nanostructure ($NaNbO_5$) and hydrogel were conducted using a field-emission scanning electron microscope (FESEM), (Zeiss). The electrical conductivity of the Nb-Hydrogel was measured using an LCR meter (Hioki). The electrical output signals, including voltage (V), current (I), and power (P) generated by the Nb-Hydrogel, were measured using an (Aplab D37070A) oscilloscope. For current measurements, a (Keithley) electrometer was utilized.

Gas Sensing: Gas sensing studies were conducted using an indigenous gas sensing system equipped with an inbuilt heater and interfaced with a computer-controlled multimeter. The system utilized dry CO gas from Sigma gas cylinder. The computer-controlled multimeter (KM-891) served to monitor and record the electrical responses generated by the gas sensing system.

Supporting Information

Supporting Information is available from the Wiley Online Library or from the author.

Conflict of Interest

The authors declare no conflict of interest.

Data Availability Statement

The data that support the findings of this study are available from the corresponding author upon reasonable request.

Keywords

CO gas sensor, flexibility, hydrogel, mechanical energy harvesting, single-electrode triboelectric nanogenerator, stretchability

Received: May 8, 2024
Published online:

[1] D.-H. Kim, N. Lu, R. Ma, Y.-S. Kim, R.-H. Kim, S. Wang, J. Wu, S. M. Won, H. Tao, A. Islam, K. J. Yu, T.-I. Kim, R. Chowdhury, M. Ying, L. Xu, M. Li, H.-J. Chung, H. Keum, M. McCormick, P. Liu, Y.-W. Zhang, F. G. Omenetto, Y. Huang, T. Coleman, J. A. Rogers, *Science* **2011**, *333*, 838.
[2] R.-H. Kim, D.-H. Kim, J. Xiao, B. H. Kim, S.-I. Park, B. Panilaitis, R. Ghaffari, J. Yao, M. Li, Z. Liu, V. Malyarchuk, D. G. Kim, A.-P. Le, R. G. Nuzzo, D. L. Kaplan, F. G. Omenetto, Y. Huang, Z. Kang, J. A. Rogers, *Nat. Mater.* **2010**, *9*, 929.
[3] F. R. Fan, W. Tang, Z. L. Wang, *Adv. Mater.* **2016**, *28*, 4283.
[4] Y. Sun, J. A. Rogers, *Adv. Mater.* **2007**, *19*, 1897.
[5] C. Wu, X. Wang, L. Lin, H. Guo, Z. L. Wang, *ACS Nano* **2016**, *10*, 4652.
[6] I.-V. Mihai, *Chem Soc Rev* **2014**, *43*, 6470.
[7] Y. H. Jung, T.-H. Chang, H. Zhang, C. Yao, Q. Zheng, V. W. Yang, H. Mi, M. Kim, S. J. Cho, D.-W. Park, H. Jiang, J. Lee, Y. Qiu, W. Zhou, Z. Cai, S. Gong, Z. Ma, *Nat. Commun.* **2015**, *6*, 7170.
[8] Q. Zheng, Y. Zou, Y. Zhang, Z. Liu, B. Shi, X. Wang, Y. Jin, H. Ouyang, Z. Li, Z. L. Wang, *Sci. Adv.* **2016**, *2*, 1501478.
[9] Z. L. Wang, *Farad. Discuss.* **2014**, *176*, 447.
[10] Z. L. Wang, J. Chen, L. Lin, *Energy Environ. Sci.* **2015**, *8*, 2250.
[11] S. Niu, X. Wang, F. Yi, Y. S. Zhou, Z. L. Wang, *Nat. Commun.* **2015**, *6*, 8975.
[12] H. Nishide, K. Oyaizu, *Science* **2008**, *319*, 737.
[13] S. Li, J. Wang, W. Peng, L. Lin, Y. Zi, S. Wang, G. Zhang, Z. L. Wang, *Adv. Energy Mater* **2017**, *7*, 1602832.
[14] Z. Wen, Y. Yang, N. Sun, G. Li, Y. Liu, C. Chen, J. Shi, L. Xie, H. Jiang, D. Bao, Q. Zhuo, X. Sun, *Adv. Funct. Mater.* **2018**, *28*, 1803684.
[15] M. He, W. Du, Y. Feng, S. Li, W. Wang, X. Zhang, A. Yu, L. Wan, J. Zhai, *Nano Energy* **2021**, *86*, 106058.
[16] R. Wen, J. Guo, A. Yu, K. Zhang, J. Kou, Y. Zhu, Y. Zhang, B.-W. Li, J. Zhai, *Nano Energy* **2018**, *50*, 140.
[17] R. Wen, J. Guo, A. Yu, J. Zhai, Z. l. Wang, *Adv. Funct. Mater.* **2019**, *29*, 1807655.
[18] C. K. Jeong, J. Lee, S. Han, J. Ryu, G.-T. Hwang, D. Y. Park, J. H. Park, S. S. Lee, M. Byun, S. H. Ko, K. J. Lee, *Adv. Mater.* **2015**, *27*, 2866.
[19] Y. J. Fan, X. S. Meng, H. Y. Li, S. Y. Kuang, L. Zhang, Y. Wu, Z. L. Wang, G. Zhu, *Adv. Mater.* **2017**, *29*, 1603115.
[20] F.-R. Fan, Z.-Q. Tian, Z. Lin Wang, *Nano Energy* **2012**, *1*, 328.
[21] Y. Guo, X.-S. Zhang, Y. Wang, W. Gong, Q. Zhang, H. Wang, J. Brugger, *Nano Energy* **2018**, *48*, 152.
[22] Y. Wang, W. Li, Y. Xia, X. Jiao, D. Chen, *J. Mater. Chem.* **2014**, *2*, 15124.
[23] P. Katta, M. Alessandro, R. D. Ramsier, G. G. Chase, *Nano Lett.* **2004**, *4*, 2215.
[24] L. Wang, W. A. Daoud, *Adv. Energy Mater* **2019**, *9*, 1803183.
[25] T. Liu, M. Liu, S. Dou, J. Sun, Z. Cong, C. Jiang, C. Du, X. Pu, W. Hu, Z. L. Wang, *ACS Nano* **2018**, *12*, 2818.
[26] T. Huang, C. Wang, H. Yu, H. Wang, Q. Zhang, M. Zhu, *Nano Energy* **2015**, *14*, 226.
[27] X. Pu, M. Liu, X. Chen, J. Sun, C. Du, Y. Zhang, J. Zhai, W. Hu, Z. L. Wang, *Sci. Adv.* **2017**, *3*, 1700015.
[28] L. Sun, S. Chen, Y. Guo, J. Song, L. Zhang, L. Xiao, Q. Guan, Z. You, *Nano Energy* **2019**, *63*, 103847.
[29] Q. Guan, G. Lin, Y. Gong, J. Wang, W. Tan, D. Bao, Y. Liu, Z. You, X. Sun, Z. Wen, Y. Pan, *J. Mater. Chem.* **2019**, *7*, 13948.
[30] T. B. H. Schroeder, A. Guha, A. Lamoureux, G. VanRenterghem, D. Sept, M. Shtein, J. Yang, M. Mayer, *Nature* **2017**, *552*, 214.
[31] M. T. Rahman, M. S. Rahman, H. Kumar, K. Kim, S. Kim, *Adv. Funct. Mater.* **2023**, *33*, 2303471.
[32] A. K. Bajpai, J. Bajpai, S. N. Soni, *eXPRESS Polym. Lett.* **2008**, *2*, 26.
[33] T.-Y. Ke, H.-A. Chen, H.-S. Sheu, J.-W. Yeh, H.-N. Lin, C.-Y. Lee, H.-T. Chiu, *J. Phys. Chem.* **2008**, *112*, 8827.
[34] J. H. Jung, M. Lee, J.-I. Hong, Y. Ding, C.-Y. Chen, L.-J. Chou, Z. L. Wang, *ACS Nano* **2011**, *5*, 10041.

[35] M. Mendoza, M. A. Rahaman Khan, M. A. Ishtiaque Shuvo, A. Guerrero, Y. Lin, *ISRN Nanomater.* **2012**, *2012*, 1.
[36] F. Luo, B. Chen, X. Ran, W. Ouyang, Y. Yao, L. Shang, *Nano Energy* **2023**, *118*, 109035.
[37] Z. Ma, W. Shi, K. Yan, L. Pan, G. Yu, *Chem. Sci.* **2019**, *10*, 6232.
[38] D. Bao, Z. Wen, J. Shi, L. Xie, H. Jiang, J. Jiang, Y. Yang, W. Liao, X. Sun, *J. Materials Chemistry A* **2020**, *8*, 13787.
[39] Y.-C. Lai, J. Deng, S. Niu, W. Peng, C. Wu, R. Liu, Z. Wen, Z. L. Wang, *Adv. Mater.* **2016**, *28*, 10024.
[40] H. Shaukat, A. Ali, S. Bibi, S. Mehmood, W. A. Altabey, M. Noori, S. A. Kouritem, *Energy Reports* **2023**, *9*, 4306.
[41] W. Qian, W. Yang, Y. Zhang, C. R. Bowen, Y. Yang, *Nanomicro Lett* **2020**, *12*, 149.
[42] K. Parida, V. Bhavanasi, V. Kumar, R. Bendi, P. S. Lee, *Nano Res.* **2017**, *10*, 3557.
[43] L. Wang, W. A. Daoud, *Nano Energy* **2019**, *66*, 104080.
[44] X. Jing, H. Li, H.-Y. Mi, P.-Y. Feng, X. Tao, Y. Liu, C. Liu, C. Shen, *ACS Appl. Mater. Interfaces* **2020**, *12*, 23474.
[45] W. Xu, L. Huang, M. Wong, L. Chen, G. Bai, J. Hao, *Adv. Energy Mater* **2017**, *7*, 1601529.
[46] X. Luo, L. Zhu, Y. Wang, J. Li, J. Nie, Z. L. Wang, *Adv. Funct. Mater.* **2021**, *31*, 2104928.
[47] Y. Luo, M. Yu, Y. Zhang, Y. Wang, L. Long, H. Tan, N. Li, L. Xu, J. Xu, *Nano Energy* **2022**, *104*, 107955.
[48] J. Yang, J. An, Y. Sun, J. Zhang, L. Zu, H. Li, T. Jiang, B. Chen, Z. L. Wang, *Nano Energy* **2022**, *97*, 107199.